Mechanistic analysis of an IRF7-dependent pathway in virus-induced fibrosis in chronic lung allograft dysfunction

Mudassir M. Banday,[a,e,g] Mizanur Rahman,[a,g] Yasufumi Goda,[a,e] Andrew S. Potter,[b] Tatsuhiko Naito,[c] Haripriya Mallidi,[a] Ranu Surolia,[d] Stefi Lee,[a,f] Rakhshinda Rehman,[a] Gabriel Loor,[e] Don Hayes, Jr.[b] and Nirmal S. Sharma[a,e,f,*]

[a]Brigham and Women's Hospital, Harvard Medical School, Boston, MA, USA
[b]Cincinnati Children's Hospital Medical Center, University of Cincinnati College of Medicine, OH, USA
[c]Medical Support Center for the Japan Environment and Children's Study, National Center for Child Health and Development, Tokyo, Japan
[d]University of Alabama at Birmingham Heersink School of Medicine, Birmingham, AL, USA
[e]Baylor College of Medicine, Houston, TX, USA
[f]VA West Roxbury, Medical Center, Boston, MA, USA

eBioMedicine
2026;128: 106285
Published Online xxx
https://doi.org/10.1016/j.ebiom.2026.106285

Summary

Background Chronic lung allograft dysfunction (CLAD) significantly limits long-term survival of lung transplant recipients, with viral infections acting as critical contributors to its pathogenesis. The mechanisms linking viral infections to CLAD-associated airway fibrosis remain incompletely understood. This study investigates the role of the type I interferon (IFN) master regulator IRF7 in virus-induced airway fibrogenesis.

Methods CLAD (Bronchiolitis obliterans syndrome (BOS)), Stable LTx, and non-transplanted lung tissues were analysed by spatial transcriptomics (GeoMx; n = 5 CLAD (BOS), n = 3 Stable LTx, n = 3 controls), Western blotting, and immunostaining. Primary bronchial epithelial cells in air-liquid-interface (ALI) culture and a human precision-cut lung slice (PCLS) *ex vivo* model were exposed to Influenza A virus (IAV) with or without IRF7 silencing, IL-33 blockade, or MMP-9 inhibition. Group comparisons used Mann–Whitney tests and one-way ANOVA with Tukey's post hoc test; spatial differential expression used linear models with Benjamini–Hochberg correction ($\alpha = 0.05$).

Findings Spatial transcriptomics identified enrichment of IFN-stimulated genes including IRF7, STAT1, IFI44L, and GBP1 in the CLAD (BOS) epithelial compartment alongside antiviral effector genes (DDX58, TLR3) and pro-fibrotic programmes (TGFB1, SMAD2/3, ACTA2). Western blotting confirmed significantly increased IRF7 and phosphorylated IRF7 with airway-centric distribution in CLAD (BOS) ($p < 0.01$; n = 3–4). IAV exposure upregulated IRF7, α-SMA, SMAD2/3, and soluble collagen in ALI cultures (all $p < 0.01$; n = 3–6); IRF7 silencing attenuated these markers and reduced virus-induced IL-33 at mRNA and protein levels ($p < 0.05$). IL-33 blockade independently reduced α-SMA ($p < 0.05$), confirming IL-33 as a downstream IRF7 mediator. IAV increased MMP-9 secretion ($p < 0.0001$); IRF7 or IL-33 blockade attenuated MMP-9, while MMP-9 inhibition reduced α-SMA ($p < 0.0001$). All findings were replicated in human PCLS ($p < 0.05$; n = 5–6).

Interpretation These findings delineate an IRF7–IL-33–MMP-9 axis linking viral infections to airway fibrogenesis, offering mechanistic insight into CLAD (BOS) pathogenesis. Therapeutic targeting of this pathway may mitigate fibrotic remodelling in lung transplant recipients.

Funding NIH 1R01HL161620 (N.S.S.). Caredx IIT (N.S.S).

Keywords: Chronic lung allograft dysfunction; Bronchiolitis obliterans syndrome; Lung transplantation; Interferon regulatory factors; Fibrogenesis

*Corresponding author. Lung Transplantation Program, Division of Pulmonary and Critical Care, Baylor College of Medicine, Houston, TX, USA.
E-mail address: nirmal.sharma@bcm.edu (N.S. Sharma).
[g]Equal contribution.

Research in context

Evidence before this study

We searched PubMed, Embase, Web of Science, and bioRxiv/medRxiv from Jan 1, 2000 to Sept 18, 2025 (no language limits), and hand-searched reference lists. Terms included "lung transplant*", "CLAD", "bronchiolitis obliterans", "viral infection", "type I interferon", "IRF7", "IL-33", "MMP-9", "epithelium", and "spatial transcriptomics". Prior work linked antiviral/IFN signalling with epithelial injury and remodelling, but direct causal data connecting IRF7 to an IL-33–MMP-9 pathway in human allografts were lacking; spatial studies were few, small, and largely descriptive.

Added value of this study

Using human transplant tissue with concise spatial profiling plus orthogonal functional models (virus-injury ALI and human PCLS), we identify and intervene on an IRF7-IL-33-MMP-9 axis driving epithelial inflammation and profibrotic remodelling relevant to CLAD (BOS). Genetic/pharmacologic modulation of pathway nodes attenuates key inflammatory and matrix-remodelling readouts, moving beyond association and towards causality.

Implications of all the available evidence

Findings support a translational framework in which transient modulation of IRF7/IL-33/MMP-9 after viral injury may reduce airway remodelling and CLAD(BOS) risk. This axis yields candidate airway biomarkers for risk stratification and druggable targets compatible with post-transplant care, motivating prospective biomarker-guided studies and early-phase trials to preserve long-term graft function.

Introduction

Lung transplantation remains the only curative therapy for patients with end-stage lung diseases who are deemed candidates, yet long-term survival is curtailed by chronic lung allograft dysfunction (CLAD), affecting more than half of recipients within five years.[1–3] Importantly, pulmonary viral infections, particularly cytomegalovirus (CMV) and community-acquired respiratory viruses including influenza, respiratory syncytial virus and human metapneumovirus among others, as key contributors to CLAD onset.[4–6] These viral pathogens inflict direct cytopathic injury on the graft and precipitate exuberant host inflammation leading to acute lung injury and activating downstream fibrogenesis.[7,8] However, the molecular circuitry that links host-viral response to progressive airway fibrosis is not well delineated.

Type I interferons (IFNs) coordinate first-line antiviral defence, with interferon-regulatory factor-7 (IRF7) acting as the master transcriptional amplifier of this pathway.[9,10] Paradoxically, chronic IRF7 activation has been associated with extracellular matrix deposition and fibrotic remodelling in lung disease,[11,12] suggesting a double-edged role in tissue repair. Downstream, the epithelial alarmin interleukin-33 (IL-33) is induced by viral infections and can propagate epithelial-to-mesenchymal transition and extracellular-matrix turnover via matrix metalloproteinase-9.[13–15] Whether an IRF7-driven IL-33/MMP-9 axis underlies virus-induced airway fibrosis in lung allografts has not been explored.

Here, we combine spatial transcriptomics of CLAD-afflicted lung explants, *in vitro* air–liquid interface epithelial model, and *ex vivo* precision-cut lung slices (PCLSs) exposed to influenza A to test the hypothesis that viral infection activates an IRF7-dependent IL-33/MMP-9 feed-forward loop that drives airway fibrogenesis and contributes to CLAD (BOS). Defining this pathway may reveal therapeutic windows in which targeted IRF7 inhibition preserves antiviral immunity while attenuating profibrotic signalling.

Methods

Ethics

The study was approved by the Institutional Review Board at Massachusetts General-Brigham (MGB) (IRB#2022P000210) and University of South Florida (Pro00032158). Demographics and characteristics of the study participants are presented in Supplementary Tables S1 and S2. Written informed consent was provided by all participants. This study was conducted in accordance with the ethical principles of the Declaration of Helsinki.

Subjects, and human specimens

Lung tissue used for our spatial transcriptomics includes (1) explanted allograft tissue from lung transplant recipients undergoing repeat transplantation for CLAD-bronchiolitis obliterans syndrome phenotype (CLAD-BOS), (2) transbronchial biopsies (from patients with no CLAD at 5 years post-lung transplant and no prior episodes of acute rejection, or antibody mediated rejection (hence referred as stable LTx), (3) lung tissues from non-transplanted organ donors (hence referred to as controls). For the *in vitro* experiments, we utilised CLAD explant tissues (re-transplantation of CLAD-BOS subjects) and Stable LTx (from autopsy of Stable LTx recipients with non-lung related deaths, details in Supplementary Table S1). The pathology core processed both CLAD explants and control specimens using the same processing protocol. These lung tissues were processed and used for downstream experiments using previously published methodology.[9]

GeoMX digital spatial profiling

Using our previously published methodology,[16,17] paraffin-embedded tissues (CLAD (BOS) n = 5, Stable LTx n = 3 and controls, n = 3) were processed and analysed using a combination of fluorescently labelled antibodies, anti-CD31, PanCK, CD45 (Supplementary Table S3). Selection of regions of interest (ROI, 9–12 per patient) was performed using immunofluorescent staining, the cellular immunofluorescent profile, and the pathological features of CLAD observed in the H&E-stained sections based on established protocol.[18] Sequencing with the Nanostring GeoMx platform was performed on the RNA probe tag and not on the transcript itself, providing less sequencing bias and a more accurate transcript count. Downstream biostatistical analyses were conducted on the total spatial transcriptome (unsegmented), compartments and details are provided in statistical analyses section below and in the Supplementary Text. Portions of the spatial transcriptomic cohort analysed in this study were included in our prior publication describing AP-1–associated transcriptional programmes in chronic lung allograft dysfunction (CLAD).[18] The present study addresses a distinct biological question focused on epithelial interferon/IRF7 signalling and incorporates additional mechanistic validation experiments.

Generation of precision-cut lung slices, infection exposure and shRNA silencing

Control lungs were used to generate PCLS using previously published methodology.[19] Sections were revived in DMEM supplemented with antibiotics and grown for 72 h, when virus (A/Hong Kong/8/1968 H3N2, ATCC) in MOI of 1.0 was added for 7 days. IRF7 shRNA plasmid complete kit (Origene, cat. TR315487) was used to suppress IRF7 expression in PCLS and were transfected with either IRF7-specific or control shRNA plasmid in the absence of antibiotics in the culture media. After 3 days of transfection, IRF7 expression was assessed using immunofluorescence microscopy.

Generation of air-liquid interface epithelial cell culture model

PBECs (Lonza, Catalogue CC-2540) were cultured in BGEM medium, transfected with IRF7-specific or control shRNA, and IRF7 knockdown was confirmed by Western blot. Cells were seeded onto 12-well transwells (0.4 μm, Sigma–Aldrich) and, after reaching confluency, differentiated at the air-liquid-interface (ALI) using PneumaCult ALI medium (STEMCELL Technologies). After two weeks, cultures were either mock-treated or infected with H3N2 virus every other day for one week. Supernatants were collected, and soluble collagen was quantified using the Sircol Assay (Biocolour).

Immunofluorescence and trichome staining

PCLS and ALI sections were immunostained following PBS washes and overnight incubation at 4 °C with antibodies against IRF7, α-SMA, MUC5AC, and H3N2 haemagglutinin (HA) in blocking buffer. Sections were then incubated with secondary antibodies: anti-rabbit IgG Fab2 Alexa Fluor® 488 (Cell Signalling), goat anti-mouse IgG Alexa Fluor® 594 (Abcam), and donkey anti-goat IgG Alexa Fluor Plus 594. Mounting was performed with VECTASHIELD® Antifade with DAPI (Vector Labs). Fluorescent images were acquired using an Olympus VS120 microscope at 40X for ALI and 25X for PCLS and analysed in FIJI-ImageJ. PCLS were stained with the Abcam Trichrome Staining Kit (ab150686). Images were deconvoluted and thresholded in ImageJ to quantify the stained area. For immunofluorescence quantification, 3–4 image fields per patient were acquired to capture all visible airways and averaged to yield a single value per biological specimen. Details of antibodies are provided in Supplementary Table S3.

Western blotting and real time PCR

Proteins from cell lysates were separated by SDS-PAGE, transferred to PVDF membranes, and probed with specific primary and HRP-conjugated secondary antibodies. Bands were visualised using a gel documentation system, and densitometry was performed with ImageJ, normalised to GAPDH. For gene expression analysis, RNA from virus-treated IRF7-shRNA and control PBECs was reverse transcribed, and qPCR was performed using SYBR Green. Relative expression was calculated using the $2^{-\Delta\Delta Ct}$ method. Antibody (Supplementary Table S3) and primer (Supplementary Table S4) details are provided in the Supplementary Text.

MMP-9 ELISA

Processed ALI culture supernatants in the lower compartment of 12 well trans well plates treated with virus (H3N2) in presence or absence of MMP-9 blocker and anti ST2 were harvested and quantified for with Human MMP-9 ELISA Kit - Quantikine (Catalogue # DMP900) using the Manufacturer's instructions.

Statistics

For statistical testing of experimental data, normality was assessed by the Shapiro–Wilk test followed by an unpaired t-test or Mann–Whitney test for two-group comparisons, or one-way ANOVA with Tukey's multiple comparison post-test for analyses involving more than two groups. A 2-tailed alpha cutoff of 0.05 was used for statistical significance. For GeoMx spatial transcriptomic analyses, ROIs were excluded if they exhibited less than 80% sequencing alignment, 50% sequencing saturation, or fewer than 100 nuclei. Outlier probes were identified using Grubbs' test. The limit of quantification (LOQ) was defined as two geometric standard deviations above the geometric mean of negative probes. Segments with a gene detection rate of less than 10% were excluded from further analysis, and

genes were filtered if their counts fell below the LOQ in at least 10% of the remaining segments.

Raw transcript counts were normalised using the 75th percentile (Q3) method and subsequently $\log_2$ transformed. Differential gene expression (DGE) between CLAD (BOS), Stable LTx, and controls was performed using the limma linear modelling framework. To account for technical variation across the cohort, slide-to-slide variation was incorporated as a blocking factor in the design matrix. Empirical Bayes moderation was applied using the eBayes function to identify significant differentially expressed genes (DEGs). Genes were considered significant at a Benjamini-Hochberg adjusted $p < 0.05$. For volcano plot highlighting and pathway visualisation, an additional absolute $\log_2$ fold change threshold of >0.5 was utilised to prioritise biologically relevant candidates. Functional enrichment and pathway analysis were conducted using clusterProfiler and Enrichr, querying the KEGG 2021, GO Biological Process, and Reactome databases. Likewise, for validation purposes Single-cell RNA sequencing data from CLAD and control lung transplant recipients were obtained from the Gene Expression Omnibus (GEO; accession GSE224210).[20]; BAM files were converted to FASTQ format using the 10× Genomics bamtofastq utility and processed with Cell Ranger (v5.0.1, 10× Genomics). SoupX was used to estimate ambient RNA and adjust counts; Seurat objects were created from the corrected count matrices, retaining cells with >500 features and >800 UMI, <20% mitochondrial reads, and <2.5% haemoglobin gene expression (HBA1, HBB). scDblFinder was used to identify and remove doublets. Data were normalised, variable features selected and PCA performed. Samples were merged into a Seurat object. Cell types were annotated using a previously published dataset[21] using the Seurat FindTransferAnchors and TransferData functions. For pathway analysis, two epithelial cell subsets were defined: (1) club and ciliated cells, and (2) all epithelial cell types (club, ciliated, alveolar type 1, alveolar type 2, goblet, mucous, ionocyte, basal, differentiating basal, proliferating basal, and proximal basal cells). Within each subset, differential gene expression between CLAD and CTRL was assessed using the FindMarkers Seurat (v5) function (Wilcoxon) with no log2FC requirement and minimum detection rate of 5%. Genes

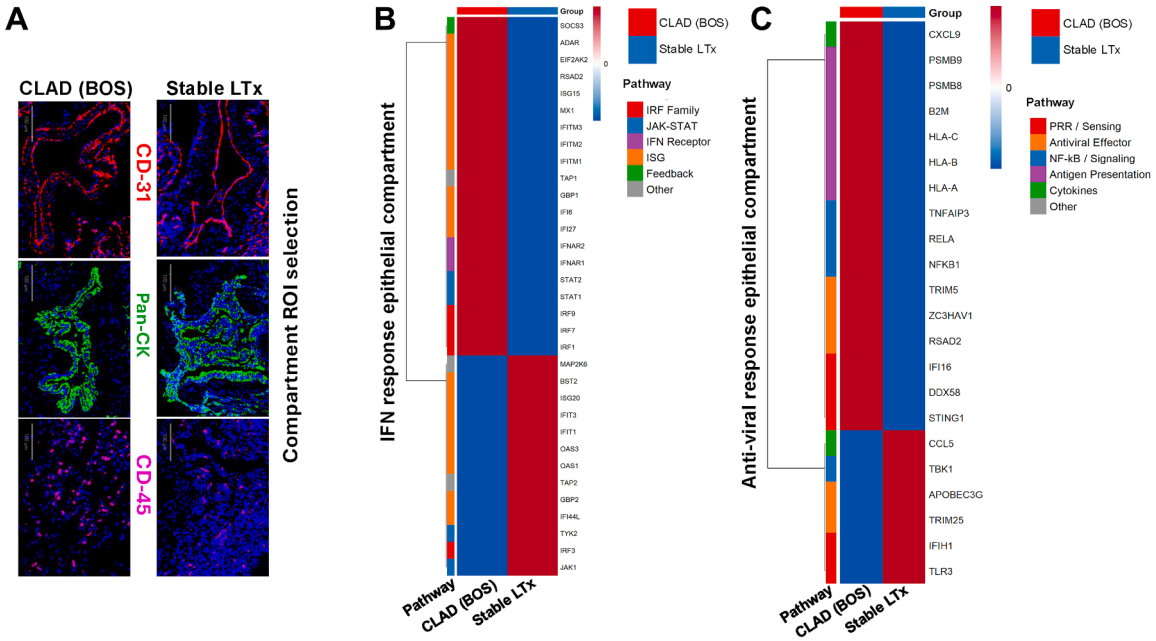

Fig. 1: **Spatial transcriptomic analysis reveals compartment-resolved enrichment of interferon-stimulated and antiviral genes in CLAD.** **(A)** Representative immunofluorescence images of compartment region of interest (ROI) selection in Stable LTx and CLAD (BOS) lung tissue sections, using CD-31 (red, endothelial), Pan-CK (green, epithelial), and CD-45 (purple, immune) markers. **(B)** Differential expression of canonical IFN-stimulated genes (ISGs) in the epithelial (Pan-CK+) compartment visualised using hierarchical clustering. CLAD (BOS) samples show distinct enrichment of type I interferon (IFN) signature genes relative to Stable LTx. Pathway colour bar indicates gene family: IRF Family (blue), JAK-STAT (cyan), IFN Receptor (purple), ISG (orange), Feedback (green), Other (grey). SOCS3 upregulation in CLAD (BOS) reflects feedback inhibition of chronic IFN activation. Colour scale indicates relative gene expression (log2-transformed counts). **(C)** Differential expression of antiviral response genes in the epithelial compartment visualised using hierarchical clustering. CLAD (BOS) samples show enrichment of PRR/Sensing (red), Antiviral Effector (orange), NF-κB/Signalling (blue), Antigen Presentation (purple), Cytokines (green), and Other (grey) pathway genes relative to Stable LTx. Colour scale indicates relative gene expression (log2-transformed counts).

were ranked by average log2 fold-change, with positive values indicating higher expression in CLAD.

Pre-ranked gene set enrichment analysis (GSEA) was performed using fgsea with a minimum gene set size of 10 and a maximum of 500. Gene sets were from the Molecular Signatures Database via the msigdbr R package: all 50 Hallmark gene sets and a curated subset of Reactome pathways selected for relevance to interferon/IRF signalling, innate and adaptive immunity, fibrosis and extracellular matrix remodelling, epithelial injury, apoptosis, and inflammatory signalling. Normalised enrichment scores (NES) were computed to enable comparison across gene sets of different sizes; positive NES indicates pathway enrichment among genes upregulated in CLAD, and negative NES indicates enrichment among genes downregulated in CLAD. Statistical significance was assessed using the Benjamini-Hochberg-adjusted p-value (FDR), with thresholds of FDR <0.05 (*), FDR <0.01 (**), and FDR <0.001 (***). Results visualised as horizontal bar plots displaying the NES for the top significant pathways in each direction, with gene counts annotated within bars. Illustrations were generated using R, BioRender and Illustrator.

Role of funders

Funders had no role in study design, data collection, data analysis, interpretation, or writing of the report.

Results

Spatial transcriptomic analysis reveals enrichment of antiviral immune pathways and elevated expression of type I interferon-stimulated genes in CLAD

To determine whether antiviral immunity and specifically type I IFN signalling was dysregulated in CLAD, we performed spatial transcriptomic profiling on CLAD (BOS) explants, stable LTx transplant tissue, and controls. Compartment-specific ROIs were defined using immunofluorescence for CD31 (endothelial), Pan-CK (epithelial), and CD45 (immune cells) (Fig. 1A, Supplementary Figs. S1–S3). Gene set enrichment analysis of the total spatial transcriptome (unsegmented) revealed significant upregulation of several immune and fibrotic pathways in CLAD compared to Stable LTx tissue, including TNF signalling, IL-17 signalling, AGE–RAGE signalling, and NF-κB signalling, alongside pathways related to antiviral immunity (Supplementary Fig. S4). More granular compartment-

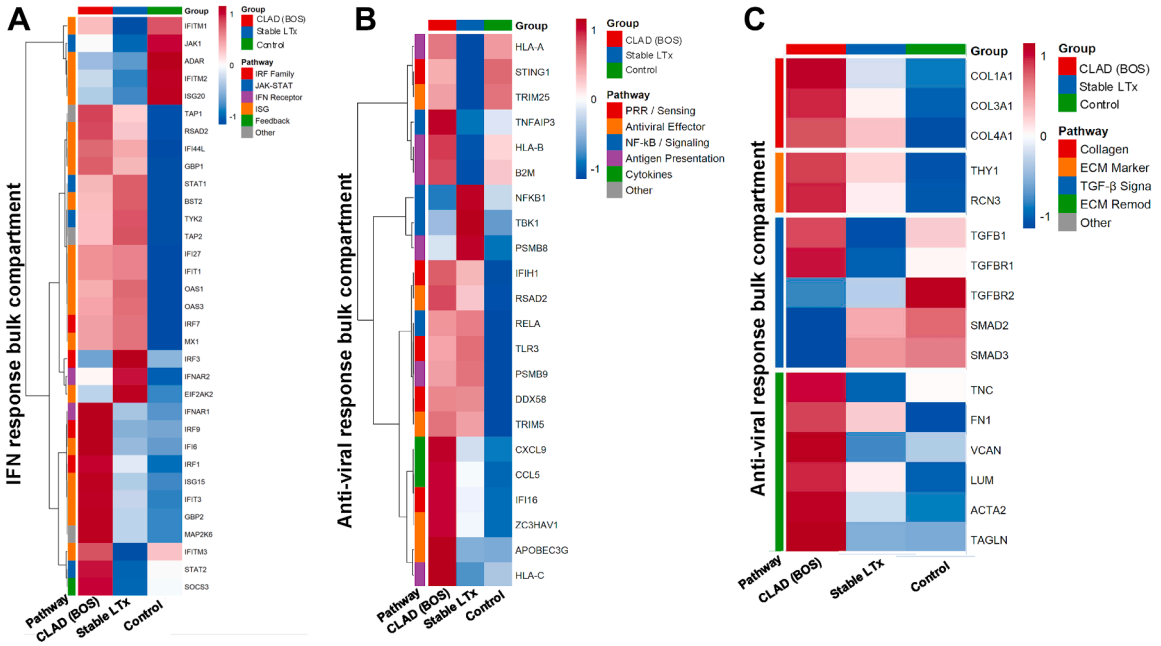

Fig. 2: **IFN response, antiviral, and fibrotic gene programmes are enriched in the bulk spatial compartment in CLAD (BOS). (A)** Heatmap showing differential expression of IFN response genes in the bulk compartment across CLAD (BOS), Stable LTx, and control groups. Pathway colour bar indicates gene family: IRF Family (blue), JAK-STAT (cyan), IFN Receptor (purple), ISG (orange), Feedback (green), Other (grey). Colour scale indicates relative gene expression (log2-transformed counts). **(B)** Heatmap showing differential expression of antiviral response genes in the bulk compartment across CLAD (BOS), Stable LTx, and control groups. Pathway colour bar indicates: PRR/Sensing (red), Antiviral Effector (orange), NF-κB/Signalling (blue), Antigen Presentation (purple), Cytokines (green), Other (grey). Colour scale indicates relative gene expression (log2-transformed counts). **(C)** Heatmap showing differential expression of fibrotic pathway genes in the bulk compartment across CLAD (BOS), Stable LTx, and control groups. Pathway colour bar indicates: Collagen (red), ECM Marker (orange), TGF-β Signalling (blue), ECM Remodelling (green), Other (grey). Colour scale indicates relative gene expression (log2-transformed counts).

resolved analysis demonstrated marked enrichment of type I IFN-stimulated genes (ISGs) in the epithelial compartment of CLAD, including IRF7, IRF1, IRF9, STAT1, IFI44L, IFI27, and GBP1, consistent with an activated type I IFN response (Fig. 1B). Distinct antiviral effector genes including RSAD2, DDX58, ZC3HAV1, and TLR3 were similarly enriched in the CLAD epithelial compartment, suggesting active innate viral sensing (Fig. 1C). SOCS3, a known negative regulator of JAK-STAT signalling, was significantly upregulated in CLAD, suggesting compensatory feedback regulation of the type I IFN response. These IFN and antiviral signatures were similarly enriched in endothelial and immune compartments in CLAD (Supplementary Fig. S5). Importantly, bulk compartment analysis also revealed upregulation of profibrotic gene programmes in CLAD, including collagens (COL1A1, COL3A1), TGF-β pathway components (TGFB1, TGFBR1/2, SMAD2/3), and ECM remodelling markers (ACTA2, FN1, VCAN), consistent with active fibrogenesis co-localising with the innate immune response (Fig. 2A–C). Further, to validate some of our observations, we conducted gene set enrichment analyses of club + ciliated epithelial cells from an independent publicly available scRNA-seq dataset (GSE224210)[20] that showed interferon and innate immune pathways significantly enriched in CLAD airway epithelium compared to controls, confirming increased IFN and innate immune signatures in epithelial cells (Supplementary Fig. S6).

Taken together, these spatial transcriptomic data demonstrate that antiviral immune activation and type I IFN signalling are broadly enriched in CLAD, and are accompanied by upregulation of profibrotic gene programmes, supporting a mechanistic link between viral immune sensing and fibrosis in CLAD.

CLAD-afflicted lungs show increased IRF7 expression

Given the increase of type 1 IFN activation in CLAD spatial transcriptomic analyses and the central role of type 1 IFN in antiviral immunity, we further explored the role of type 1 IFN master regulator IRF7 in CLAD. IRF7 is key to the activation of downstream IFN-stimulated genes.[22] To confirm whether type 1 IFN response was indeed upregulated in CLAD, we first measured the protein expression of IRF7 (as a surrogate for increased type 1 IFN response) along with the active form of IRF7 and phosphorylated IRF7 (pIRF7) in CLAD and Stable LTx whole lung lysates. Western blot analyses showed increased IRF7 ($p < 0.01$,

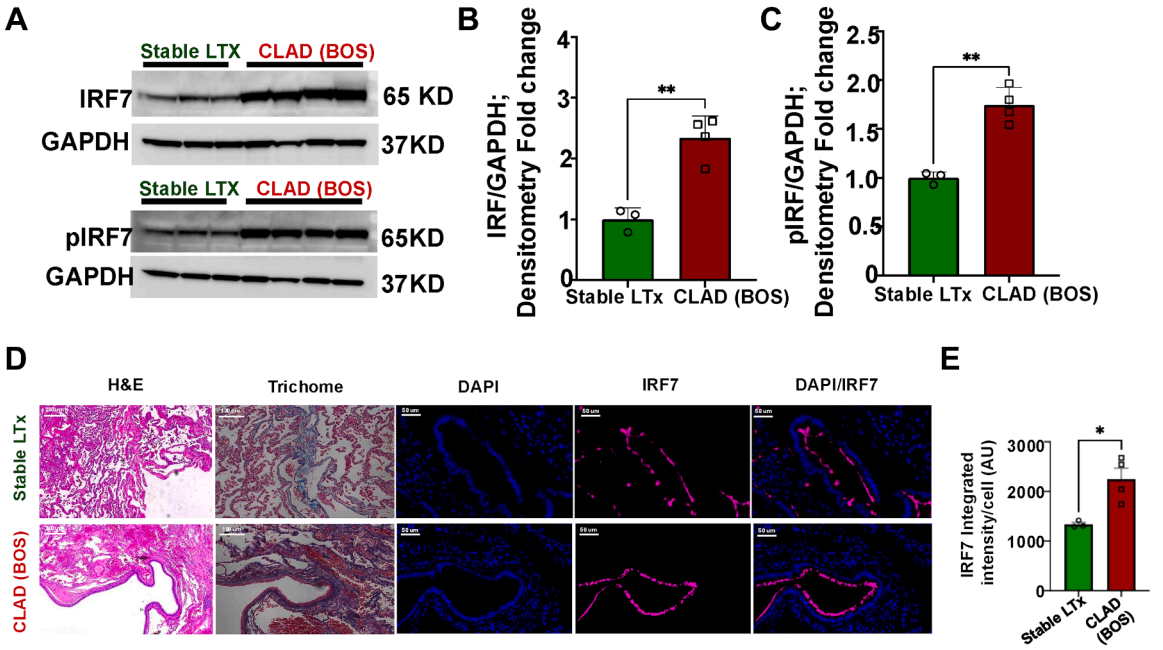

***Fig.* 3: IRF7 and pIRF7 are increased in human CLAD (BOS). (A)** Representative Western blot images showing IRF7 and pIRF7 in CLAD (BOS) and Stable LTx whole lung lysates. Densitometric analyses of the above blots (fold change relative to Stable LTx) showing protein expression of **(B)** IRF7 and **(C)** pIRF7 in CLAD (BOS) and Stable LTx whole lung tissue (Stable LTx n = 3, CLAD (BOS) n = 4). Error bars represent mean ± SEM. **p < 0.01, unpaired t-test. **(D)** Representative immunofluorescence images showing H&E, Trichrome, DAPI (blue), IRF7 (magenta), and merged DAPI/IRF7 channels in Stable LTx and CLAD (BOS) lung tissue sections, demonstrating airway-centric distribution and increased IRF7 expression in CLAD (BOS). **(E)** Corresponding Integrated Intensity/cell of IRF7 in human CLAD (BOS) and Stable LTx specimens. Each data point represents the mean integrated IRF7 intensity/cell averaged across 3–4 image fields per patient (Stable LTx n = 3, CLAD (BOS) n = 4); group data presented as mean ± SEM; *p = 0.017, unpaired t-test.

unpaired t test) and pIRF7 expression ($p < 0.01$, unpaired t test) in CLAD (Fig. 3A–C). Next, to localise the distribution of IRF7 in the lung, we conducted immunostaining. Our results demonstrated an airway-centric distribution and increased IRF7 expression in CLAD ($p = 0.017$, unpaired t test) (Fig. 3D). Antibody specificity for IRF7 immunofluorescence was confirmed by secondary-only controls, and increased pIRF7 expression in CLAD was further validated by immunohistochemistry (Supplementary Fig. S7).

Virus exposure induces IRF7 expression and fibrogenesis, while IRF7 silencing attenuates it

Type 1 IFN responses are key to viral immunity; however, their activation can also impact downstream profibrotic and pro-inflammatory signalling pathways.[23,24] Emerging literature has implicated a role for IRF7 in fibrosis.[25,26] As a proof of concept, we used Influenza A (IAV) to delineate the impact of viruses on IRF7 activation and downstream fibrogenesis. We used an ALI primary bronchial epithelial cell (PBEC) model to mirror the airway epithelium and explore the role of viruses on IRF7 activation and fibrogenesis. Exposure to IAV resulted in significant upregulation of IRF7 ($p < 0.01$, one-way ANOVA with Tukey's multiple comparison test) and key fibrotic markers, including aSMA, SMAD 2/3, and collagen (Fig. 4A–E). To determine whether IRF7 was contributory to ongoing fibrogenesis, we conducted shRNA-mediated IRF7 silencing followed by IAV exposure. We detected a significant reduction in fibrogenesis with IRF7 silencing (Fig. 4A and B), as evidenced by reduced aSMA ($p < 0.01$, Mann–Whitney U test), SMAD 2/3 ($p < 0.05$, Mann–Whitney U test), and collagen ($p < 0.01$, Mann–Whitney U test) (Fig. 4C–E). Further IRF silencing also attenuated airway mucogenesis (MUC5AC expression) in our ALI model (Fig. 4F). Next, to validate and elucidate its human translational relevance, we repeated the same exposures in a human PCLS *ex vivo* model, in which airway (β-tubulin+) and vascular (vWF+) compartments were confirmed by immunofluorescence (Supplementary Fig. S8). Viral infection of PCLS was confirmed by haemagglutinin (HA) immunofluorescence (Supplementary Fig. S9). Similar to our ALI model, IAV exposure significantly upregulated IRF7 ($p < 0.01$, Mann–Whitney U test) and activated fibrogenic markers (aSMA, $p < 0.01$, Mann–Whitney U test) (Fig. 5A and B), while IRF7 blockade (Fig. 5C) attenuated the development of fibrosis (Collagen-Trichome staining), $p < 0.05$,

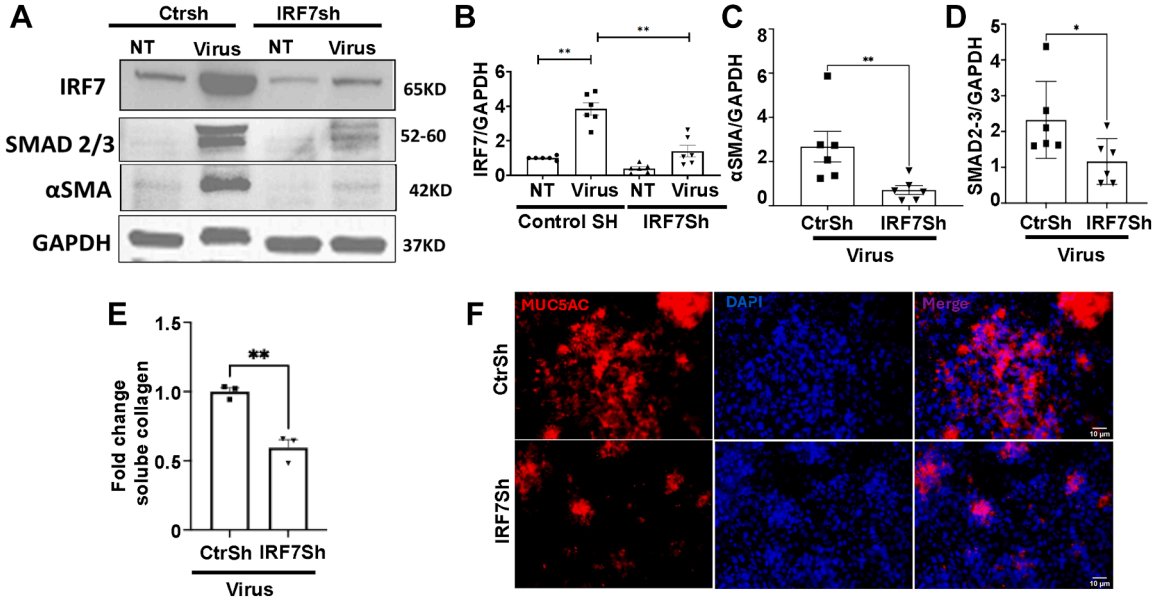

Fig. 4: **Virus exposure induces IRF7 and airway fibrogenesis in the air-liquid-interface PBEC model, and IRF7 silencing attenuates it. (A)** Representative Western blots showing protein expression of IRF7, α-SMA, and SMAD2/3 in stably expressing control (Ctr) shRNA and IRF7 shRNA primary bronchial epithelial cell (PBEC) cell line air-liquid-interface (ALI) cultures in the presence and absence of Influenza A virus (IAV). Densitometric analyses of the above blots showing protein expression of **(B)** IRF7, **(C)** α-SMA, and **(D)** SMAD2/3 in Ctr shRNA and IRF7 shRNA PBEC cell line ALI cultures (n = 6 each). Error bars represent mean ± SEM. *p < 0.05, **p < 0.01, Mann–Whitney test for 2 samples, one way Anova with Tukeys multiple comparison test for >3 groups **(E)** Sircol assay showing fold change soluble collagen content in the ALI culture supernatants from the above experiments (n = 3 each). Error bars represent mean ± SEM. **p < 0.01, Mann–Whitney test. **(F)** Representative immunofluorescence images showing DAPI (blue) and MUC5AC (red) of stably expressing control shRNA and IRF7 shRNA cell line ALI cultures exposed to IAV, demonstrating attenuation of airway mucogenesis with IRF7 silencing.

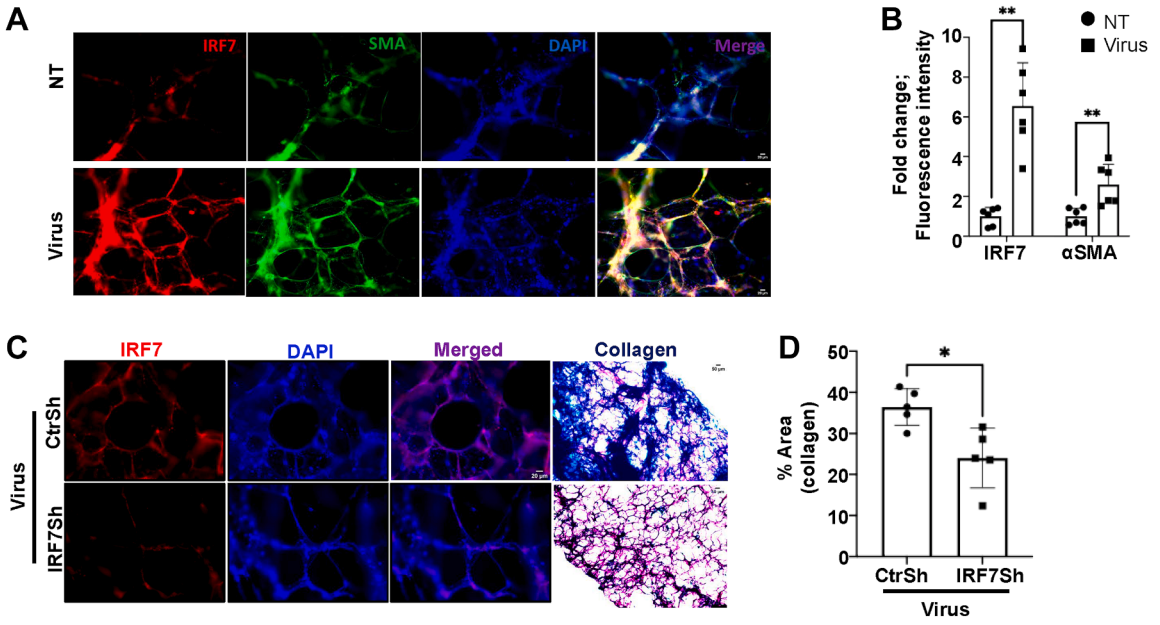

Fig. 5: **Virus exposure induces fibrogenesis and IRF7 blockade attenuates it in the human precision-cut lung slice *ex vivo* model. (A)** Representative immunofluorescence images showing IRF7 (red), α-SMA (green), DAPI (blue), and merged channels in a human precision-cut lung slice (PCLS) model in non-treated (NT) and Influenza A virus (IAV)-exposed conditions. **(B)** Corresponding fold change fluorescence intensity of IRF7 and α-SMA in the above experiment (n = 5–6 each). Error bars represent mean ± SEM. **p < 0.01, Mann–Whitney test. **(C)** Representative immunofluorescence images showing IRF7 (red), DAPI (blue), and merged channels, alongside trichrome staining showing collagen deposition, in IAV-exposed stably expressing control shRNA and IRF7 shRNA PCLS slices. **(D)** % Area of slices positive for trichrome stain in IAV-exposed stably expressing control shRNA and IRF7 shRNA PCLS slices (n = 5–6 each). Error bars represent mean ± SEM. *p < 0.05, Mann–Whitney test.

Mann–Whitney U test (Fig. 5C and D, Supplementary Fig. S10).

Influenza a exposure induces IL-33 and IRF7 blockade attenuates it

Previously, we reported elevated levels of IL-33 in CLAD and a regulatory role for IL-33 in microbe induced airway fibrogenesis.[27] Due to IRF7 being a well-known regulator of IL-33 expression,[25] we further delineated intercurrent mechanisms by exploring the IL-33 response upon IAV exposure in our ALI model and identified IL-33 induction ($p < 0.05$, one way Anova, with Tukey's multiple correction test) occurred with viral exposure (Fig. 6A and B). To decipher whether viral-induced IRF7 and IL-33 activations were interlinked, we conducted IRF7 shRNA blockade and repeated the virus exposure and found a significant reduction in IL-33 expression ($p < 0.05$, one way Anova, with Tukeys multiple correction test) at both mRNA and protein levels compared to controls, suggesting a regulatory role of IRF7 in viral-induced IL-33 production (Fig. 6A and B, Supplementary Fig. S11). Next, to determine if IL-33 was downstream of IRF7 in activation of pro-fibrotic responses, we conducted IL-33 blockade with and without IRF7 silencing in the presence of virus exposure. IL-33 blockade alone in the virus-exposed ALI model attenuated αSMA protein expression ($p < 0.05$, one way Anova, with Tukeys multiple correction test (Fig. 6C blot lane 2 and 6, Fig. 6D Bar 1 and 3). However, no significant change in αSMA protein expression with virus exposure was observed in IL-33 blockade, once IRF7 was blocked (Fig. 6C blot lane 4 and 8, Fig. 6D Bar 2 and 4) suggesting the upstream regulatory role of IRF7 in this cascade. Likewise, no significant change in αSMA protein expression was observed in virus exposed to ctrshRNA versus IRFshRNA ALI model with IL-33 blockade (Fig. 6D Bar 3 and 4). These data suggest that IL-33 is a downstream mediator to IRF7 in viral-induced fibrogenesis.

MMP-9 blockade attenuates virus-mediated fibrogenesis

Matrix metalloproteinase (MMP) 9 cleaves latent TGFb to the active form and activates the TGFb/SMAD fibrogenic axis, thus is a key contributor to lung fibrosis.[28] By directly degrading extracellular matrix and activating repair and regenerative processes, MMP-9 augments fibrogenesis.[29] Moreover, IL-33 induces and regulates MMP-9 secretion.[15,30] Taken together, we

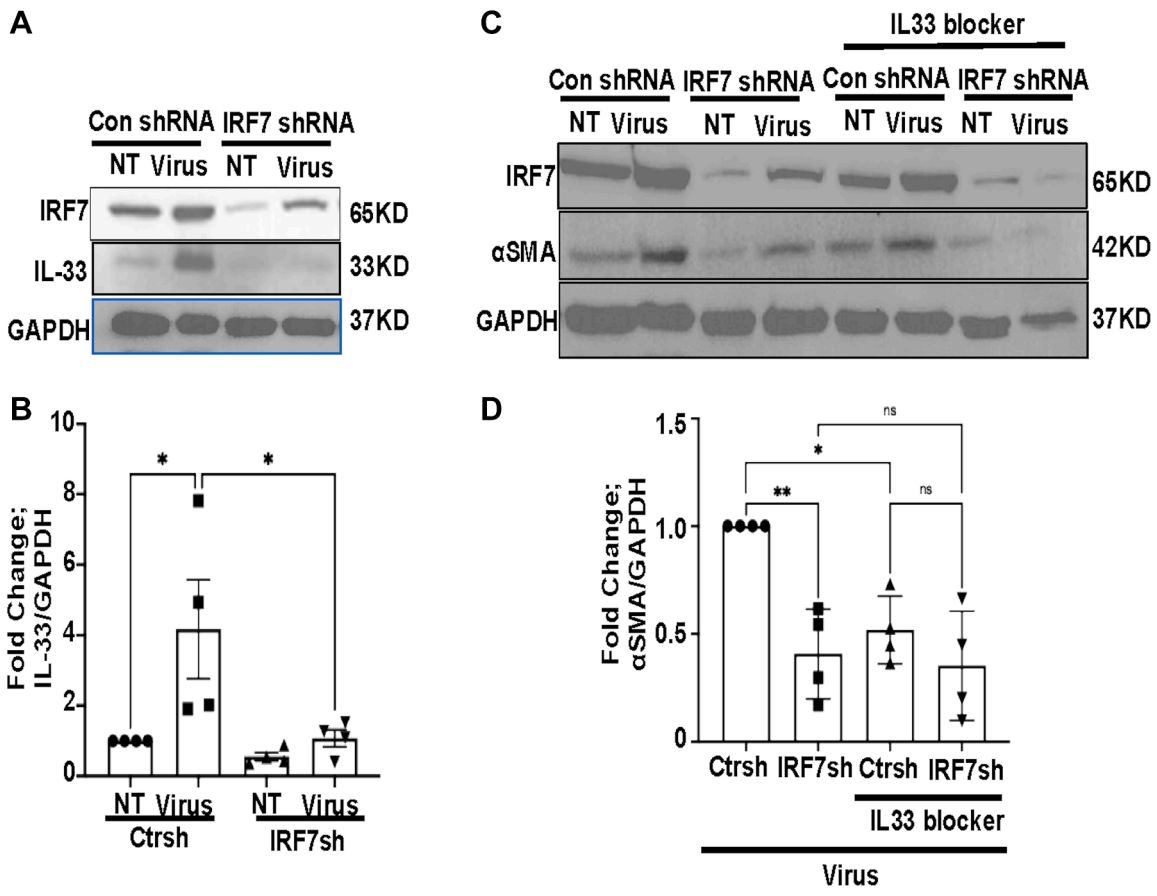

Fig. 6: **Virus induces IL-33 via IRF7 and IL-33 blockade attenuates virus-induced fibrogenesis. (A)** Representative Western blots showing protein expression of IRF7 and IL-33 in stably expressing control shRNA and IRF7 shRNA primary bronchial epithelial cell (PBEC) cell line air-liquid-interface (ALI) cultures in the presence and absence of Influenza A virus (IAV). **(B)** Densitometry fold change protein expression of IL-33 in control shRNA and IRF7 shRNA PBEC cell line ALI cultures in the presence and absence of IAV (n = 4 each). Error bars represent mean ± SEM. *p < 0.05, 1-way ANOVA with Tukey's multiple comparison post-test. **(C)** Representative Western blots showing protein expression of IRF7 and α-SMA in stably expressing control shRNA and IRF7 shRNA PBEC cell line ALI cultures in the presence and absence of IAV and IL-33 blockade. **(D)** Densitometry fold change of α-SMA protein expression in stably expressing control shRNA and IRF7 shRNA PBEC cell line ALI cultures in the presence and absence of IAV and IL-33 blockade (n = 4 each). Error bars represent mean ± SEM. *p < 0.05, **p < 0.01, ns = not significant, 1-way ANOVA with Tukey's multiple comparison post-test.

investigated mechanisms involved in viral-mediated fibrogenesis by evaluating MMP-expression after IAV exposure. We discovered MMP-9 expression increased ($p < 0.0001$, 1-way ANOVA with Tukey's multiple comparison post-test) with virus exposure (Fig. 7A, B, and D), and IRF7 or IL-33 blockade attenuated this response ($p < 0.0001$, 1-way ANOVA with Tukey's multiple comparison post-test) (Fig. 7B and C), indicating MMP-9 activation was downstream of both IRF7 and IL-33. To further delineate this pathway, we measured MMP-9 protein levels in cell culture supernatants of our IRF7-silenced ALI model exposed to IAV with and without IL-33 blockade and found no difference in secreted MMP-9 levels between the 2 groups (Fig. 7D). Therefore, our findings suggest that IRF7 is upstream of IL-33 followed by MMP-9 distally. Finally, we sought to identify whether MMP-9 was the distal mediator in viral-induced fibrogenesis. To ascertain that, we conducted MMP-9 small molecule blockade in our viral-exposed ALI model and found that MMP-9 blockade attenuated αSMA protein expression ($p < 0.01$, 1-way ANOVA with Tukey's multiple comparison post-test) (Fig. 7E and F), suggestive of MMP-9 being a distal mediator of viral-induced fibrogenesis.

Discussion

Viral exposure is a well-recognised risk factor for the development of CLAD after lung transplantation.[31] Yet, the profibrotic signals that convert acute injury into airway remodelling and fibrosis remain poorly defined. Leveraging spatial transcriptomics, explanted CLAD tissue, and complementary ALI and PCLS models of viral exposure, we delineate an IRF7-centered type I

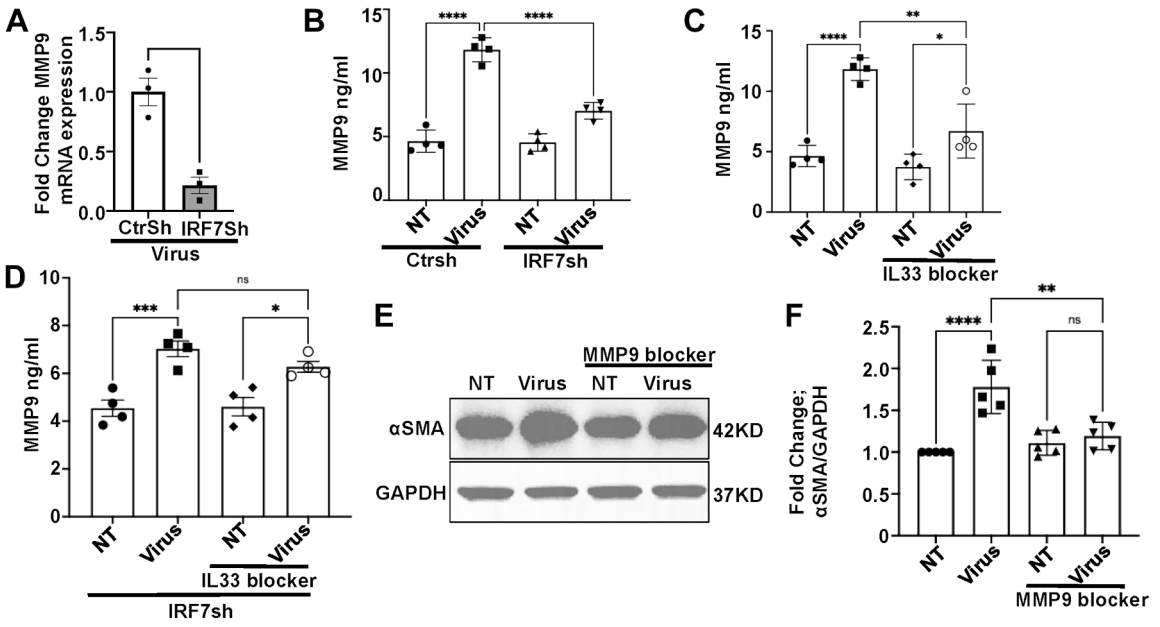

Fig. 7: **MMP-9 blockade attenuates virus-mediated fibrogenesis. (A)** Fold change mRNA expression of MMP-9 in stably expressing control shRNA and IRF7 shRNA primary bronchial epithelial cell (PBEC) cell line air-liquid-interface (ALI) cultures in the presence and absence of Influenza A virus (IAV) (n = 3 each). Error bars represent mean ± SEM. **p < 0.01, Mann–Whitney test. **(B)** MMP-9 (ng/ml of supernatant) concentrations by ELISA in the lower compartment of control shRNA and IRF7 shRNA PBEC cell line ALI culture medium in the presence and absence of IAV (n = 4 each). Error bars represent mean ± SEM. ****p < 0.0001, 1-way ANOVA with Tukey's multiple comparison post-test. **(C)** MMP-9 (ng/ml of supernatant) concentrations by ELISA in the lower compartment of IAV-exposed PBEC cell line ALI model with and without IL-33 blockade (n = 4 each). Error bars represent mean ± SEM. ****p < 0.0001, **p < 0.01, *p < 0.05, 1-way ANOVA with Tukey's multiple comparison post-test. **(D)** MMP-9 (ng/ml of supernatant) concentrations by ELISA in the lower compartment of IAV-exposed stably expressing IRF7 shRNA PBEC ALI model with and without IL-33 blockade (n = 4 each). Error bars represent mean ± SEM. *p < 0.05, ns = not significant, 1-way ANOVA with Tukey's multiple comparison post-test. **(E)** Representative Western blots showing protein expression of α-SMA in virus-exposed ALI PBEC model with and without MMP-9 blockade. **(F)** Densitometry fold change protein expression of α-SMA in IAV-exposed ALI PBEC model with and without MMP-9 blockade (n = 5 each). ****p < 0.0001, **p < 0.01, ns = not significant, 1-way ANOVA with Tukey's multiple comparison post-test.

IFN activation programme that drives the IL-33–MMP-9 cascade culminating in airway fibrosis (Fig. 8). Blocking individual nodes in this axis IRF7, IL-33, or MMP-9 attenuated collagen deposition and myofibroblast activation in our models. However, IRF7 blockade and IL-33 neutralisation did not fully normalise fibrotic markers, indicating that parallel pathways also contribute and that IRF7 represents one important component within a broader fibrogenic network.

Our transcriptomics data revealed broad enrichment of IFN-stimulated genes and the negative regulator SOCS3 in CLAD (BOS) compared with stable LTx recipients and controls, consistent with chronic type I IFN activity.[32,33] While prior work from our group using this cohort identified coordinated AP-1 activation across lung compartments, the present study extends these observations by providing mechanistic evidence that an epithelial IRF7–IL-33–MMP-9 axis links antiviral responses to airway fibrogenesis.[18] Compartment-resolved analysis further demonstrated that this IFN and antiviral immune activation was present across epithelial, endothelial, and immune cell fractions, suggesting a coordinated, tissue-wide innate immune response rather than an epithelium-restricted phenomenon. Notably, profibrotic gene programmes, including collagens, TGF-β/SMAD components, and ECM remodelling markers were co-enriched in the same spatial compartments as the IFN signature in CLAD, providing transcriptomic evidence that antiviral immune activation and fibrogenesis are spatially coupled in the allograft. Beyond the IFN/antiviral signature, our pathway analyses revealed the enrichment of TNF, IL-17, NF-κB, and AGE–RAGE pathways in CLAD explants. These pathways are typically triggered by viral sensing through innate immune receptors such as toll-like receptors (TLRs) and RIG-I-like helicases and are amplified by type I IFN signalling.[34–36] Together, they promote epithelial injury, sustained inflammation, and fibrotic remodelling. IRF7, the master amplifier of this pathway[22] was up-regulated in CLAD explants and localised predominantly to the airway epithelium, where its phosphorylated form was abundant in our analysis. Although genetic deficiencies in IRF7 can increase susceptibility to respiratory viral

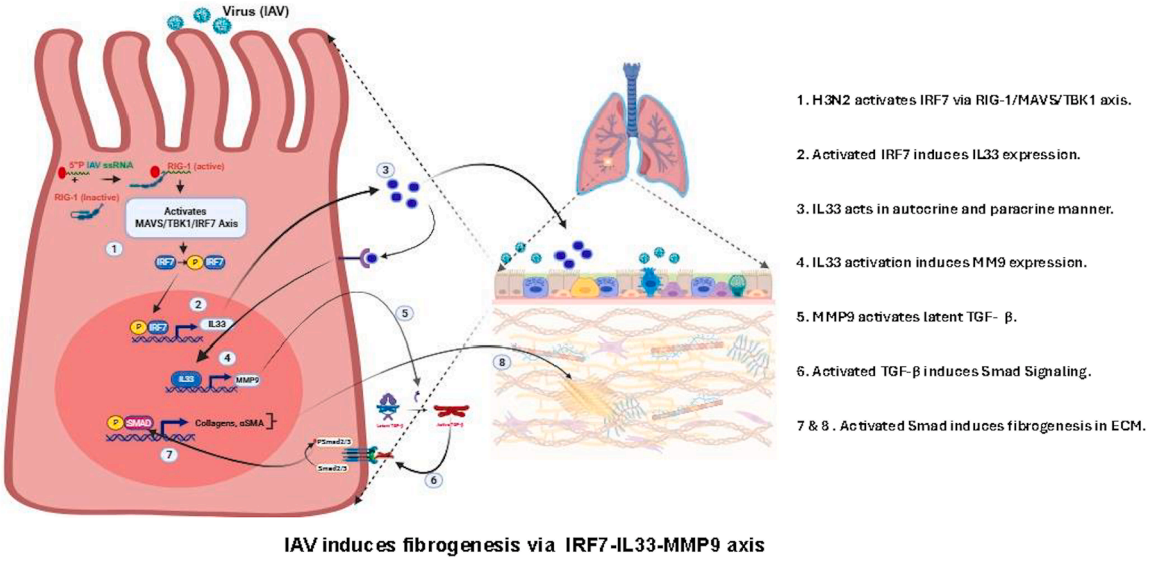

Fig. 8: **Schematic representation of the pathway involved in virus-induced airway fibrogenesis. (1 and 2)** Influenza virus activates IRF7 via the RIG-1/MAVS/TBK1 axis, and activated IRF7 enters the nucleus and induces expression of IL-33. **(3 and 4)** IL-33 is secreted from the epithelial cells into the interstitial matrix, where it acts upon neighbouring epithelial cells, resident fibroblasts, and other cell types (paracrine), as well as the same cell (autocrine manner). **(5)** IL-33 induces MMP-9 expression, and MMP-9 is secreted into the interstitial matrix. **(6)** MMP-9 cleaves latent TGF-β to its active form. **(7 and 8)** Activated TGF-β induces SMAD2/3 signalling, driving expression of collagens and α-SMA and culminating in fibrogenesis and extracellular matrix remodelling.

infections,[37] its activation is well-known to promote the formation of complexes with SMAD3 to enhance type I IFN activity, which has been implicated in the pathogenesis of fibrotic diseases including idiopathic pulmonary fibrosis (IPF) and systemic sclerosis.[22,26,38]

To elucidate the mechanisms behind virus-driven fibrogenesis, we exposed ALI cultures to IAV, which resulted in up-regulation of IRF7, α-SMA, and phosphorylated SMAD2/3 and increased soluble-collagen release. Silencing IRF7 suppressed all three read-outs, confirming its regulatory role in virus-triggered fibrogenesis. IL-33, a pleiotropic alarmin that augments antiviral responses via type I IFN signalling,[25,39] is also transcriptionally governed by IRF7.[25,40] We previously described that IL-33 accelerates airway fibrogenesis and heightens CLAD risk,[27] aligning with reports that it drives epithelial-to-mesenchymal transition in fibrosis.[15,41] IRF7 knock-down also blunted epithelial IL-33 induction; conversely, IL-33 neutralisation reduced α-SMA without additional benefit when combined with IRF7 silencing, placing IL-33 downstream of IRF7. Both IRF7 and IL-33 blockade diminished MMP-9 secretion, and pharmacologic MMP-9 inhibition further curtailed collagen accumulation, identifying MMP-9 as a distal effector. This is consistent with MMP-9 being a well-characterised mediator of extracellular matrix remodelling in fibrosis.[28,42] Importantly, incomplete normalisation of MMP-9 and α-SMA with IRF7 or IL-33 blockade alone suggests that additional pathways including direct TLR3/RIG-I–NF-κB activation, TNF-α and IL-1β-driven MMP induction, and TGF-β/MAPK signalling contribute to the residual fibrogenic response following viral injury. To establish clinical relevance, we employed a human PCLS model that preserves tissue-resident immune and structural cell.[19,43] IRF7 blockade in this model markedly reduced collagen deposition in virus-exposed PCLS, underscoring the pathway's translational significance. Together, these data support a feed-forward IRF7 → IL-33 → MMP-9 circuit that converts antiviral signalling into progressive airway remodelling. Targeting this pathway may attenuate post-viral fibrogenesis in the lung. Nonetheless, type I IFNs are indispensable for viral clearance; therapeutic modulation must be temporal rather than absolute. Future *in vivo* mechanistic work should define the precise post-infection window during which IRF7 inhibition preserves viral clearance while minimising downstream profibrotic signalling.

Data from other investigators have also identified the importance of the IRF7-IL-33-MMP-9 axis for immune activation and fibrogenesis. IRF7 promotes IL-33 release in diseases caused by autoimmunity.[25,44,45] Blocking IRF7 pathways reduced chronic fibroinflammatory responses by suppressing type I IFN responses, specifically IL-33.[46] Moreover, IL-33 blockade reduces fibrogenesis, inflammation, and MMP-9 levels in animal models of chronic injury.[15,47,48] This evidence suggests that the IRF7–IL-33–MMP-9 axis is a key contributor to fibroinflammatory processes. Alongside these findings, complementary mechanisms have been

described in CLAD including aberrant TGF-β/SMAD signalling driving myofibroblast differentiation,[49,50] TNF-α-mediated airway epithelial apoptosis,[51] and NK cell and cytotoxic CD8+ T cell accumulation promoting basal cell loss,[20,52] all of which may act in concert with or independently of the viral IRF7 axis to perpetuate airway obliteration. The relative contribution of each pathway likely varies with CLAD subtype, viral trigger, and immunosuppressive background, underscoring the need for mechanistic studies across a broader range of clinical contexts. Our data reveal a post-viral inflammatory pathway that drives fibrogenesis, suggesting that the IRF7–IL-33–MMP-9 axis may be broadly relevant to chronic fibrotic lung diseases well beyond the transplant setting.

Our study has some limitations. The spatial cohort was small and potentially subject to selection bias, as BOS-CLAD tissue was derived from patients who underwent re-transplantation; however, BOS represents the predominant CLAD phenotype (~70–80% of cases), and the limited cohort size precluded multivariate or subgroup analyses beyond CLAD vs. Stable LTx and compartment-specific comparisons. Future studies should evaluate role of IFN responses in other CLAD subtypes such as RAS and mixed phenotype. IAV was used as a model virus, which may not fully capture mechanisms driven by other relevant pathogens including community-acquired respiratory viruses and CMV. Experiments were performed without immunosuppression, and future studies should confirm pathway behaviour under clinically relevant regimens given the potential impact of calcineurin inhibitors, mTOR inhibitors, and corticosteroids on IRF7 signalling. Cross-sectional tissue sampling limits causal inference, and longitudinal studies accounting for intercurrent viral infections are needed to establish IRF7's role in CLAD progression. IRF7 knockdown and IL-33 blockade reduced but did not fully normalise MMP-9 levels, implicating parallel pathways, including TLR3/RIG-I–NF-κB, TNF-α/IL-1β, and TGF-β/MAPK in residual fibrogenic signalling. Influenza exposure in the PCLS model was applied to the entire slice rather than the airway alone, so these experiments demonstrate tissue-level engagement of the IRF7-dependent fibrogenic pathway rather than airway-restricted localisation; consistently, spatial data identified IFN and antiviral enrichment across endothelial and immune compartments as well as the epithelium, suggesting the broader innate response in CLAD extends beyond the airway and warrants further investigation. Furthermore, as HA staining was not performed in the IRF7-shRNA condition, we cannot formally exclude a modest effect of IRF7 blockade on viral replication in the PCLS model; this will be addressed in future studies.

In conclusion, we identified a pathway linking viral infections to airway fibrogenesis in CLAD, centred on IRF7 activation, IL-33 signalling, and MMP-9 activity, operating within a broader network of innate immune and fibrogenic dysregulation. Targeting the IRF7–IL-33–MMP-9 axis represents a promising but likely complementary therapeutic strategy that may reduce the fibrotic consequences of viral infections when used alongside approaches targeting parallel pathways. These findings provide a basis for future studies aimed at defining optimal therapeutic windows and combination strategies to improve long-term outcomes in lung transplant recipients.

Contributors

N.S.S., M.M.B. M.R developed concept and experiments; N.S.S., S.L. collected the samples; N.S.S., A.S.P., M.R., M.M.B, R.R, Y.G., R.S., H.M., T.N. performed experiments and analysed the data; N.S.S, D.H, G.L. performed critical review of the manuscript and revised accordingly.

All authors read and approved the final version of the manuscript. A.S.P and TN have accessed and verified the underlying spatial data. Western blot, PCLS, and immunofluorescence data were accessed and verified by MMB and MR.

Data sharing statement

Spatial Transcriptomics data deposited in GEO GSE326968.

Scripts: https://github.com/tatsuhikonaito/CLAD_NanoString.

Raw data: online and raw DEG deposited on Mendeley Data.

Sharma, Nirmal (2025), "Spatial transcript CLAD", Mendeley Data, V1, https://doi.org/10.17632/f7fzdvsp4b.1.

For any questions related to this. Please reach out to corresponding author at nirmal.sharma@bcm.edu All raw data, including Western blot, are available upon request from the above email address.

Generative AI in scientific writing

During the preparation of this work, the authors used Claude AI and ChatGPT to check grammar and spelling. The authors have reviewed and confirmed the validity of the text and take full responsibility for the content of the publication.

Declaration of interests

N.S.S: Scientific advisory board, Caredx (N.S.S), Resbiotic inc, consulting fees Sanofi, New England Donor Services and IIT grant from Caredx, Law Advisory to Keechan law and Schafer McMahon LLP. **GL:** Grant support from TransMedics Grant support, Atricure Grant support, JLH Foundation Grant support, Roderi MacDonald Foundation, consulting fees Transmedics, Leadership in Organvive. **SL:** Since the submission of the manuscript has joined Biogen as an employee. All other authors declare no further conflicts of interest.

Acknowledgements

The study was supported by NIH 1R01HL161620 (N.S.S.). Caredx IIT (N.S.S), NIEHS R01ES037611 (R.S).

Appendix A. Supplementary data

Supplementary data related to this article can be found at https://doi.org/10.1016/j.ebiom.2026.106285.

References

1 OPTN/SRTR 2022 annual data report: preface. *Am J Transplant*. 2024;24(2S1):S1–S9.
2 Belperio JA, Lake K, Tazelaar H, Keane MP, Strieter RM, Lynch JP 3rd. Bronchiolitis obliterans syndrome complicating lung or heart-lung transplantation. *Semin Respir Crit Care Med*. 2003;24(5):499–530.
3 Burton CM, Carlsen J, Mortensen J, Andersen CB, Milman N, Iversen M. Long-term survival after lung transplantation depends on development and severity of bronchiolitis obliterans syndrome. *J Heart Lung Transplant*. 2007;26(7):681–686.

4 Bennett D, Bergantini L, Ferrara P, et al. Cytomegalovirus infection is associated with development of chronic lung allograft dysfunction. *Lung*. 2022;200(4):513–522.
5 D'Orsogna L, van den Heuvel H, van Kooten C, Heidt S, Claas FHJ. Infectious pathogens may trigger specific allo-HLA reactivity via multiple mechanisms. *Immunogenetics*. 2017;69(8–9):631–641.
6 de Zwart A, Riezebos-Brilman A, Lunter G, et al. Respiratory syncytial virus, human metapneumovirus, and parainfluenza virus infections in lung transplant recipients: a systematic review of outcomes and treatment strategies. *Clin Infect Dis*. 2022;74(12):2252–2260.
7 Fan W, Gui B, Zhou X, Li L, Chen H. A narrative review on lung injury: mechanisms, biomarkers, and monitoring. *Crit Care*. 2024;28(1):352.
8 Righi I, Barone I, Rosso L, et al. Immunopathology of lung transplantation: from infection to rejection and vice versa. *Front Immunol*. 2024;15:1433469.
9 Lee AJ, Ashkar AA. The dual nature of type I and type II interferons. *Front Immunol*. 2018;9:2061.
10 Samuel CE. Antiviral actions of interferons. *Clin Microbiol Rev*. 2001;14(4):778–809. table of contents.
11 Clementi N, Ghosh S, De Santis M, et al. Viral respiratory pathogens and lung injury. *Clin Microbiol Rev*. 2021;34(3).
12 Li Y, Gao J, Wang G, Fei G. Latent cytomegalovirus infection exacerbates experimental pulmonary fibrosis by activating TGF-beta 1. *Mol Med Rep*. 2016;14(2):1297–1301.
13 Le Goffic R, Arshad MI, Rauch M, et al. Infection with influenza virus induces IL-33 in murine lungs. *Am J Respir Cell Mol Biol*. 2011;45(6):1125–1132.
14 Sun Z, Ji N, Ma Q, et al. Epithelial-mesenchymal transition in asthma airway remodeling is regulated by the IL-33/CD146 axis. *Front Immunol*. 2020;11:1598.
15 Wu L, Luo Z, Zheng J, et al. IL-33 can promote the process of pulmonary fibrosis by inducing the imbalance between MMP-9 and TIMP-1. *Inflammation*. 2018;41(3):878–885.
16 Margaroli C, Benson P, Sharma NS, et al. Spatial mapping of SARS-CoV-2 and H1N1 lung injury identifies differential transcriptional signatures. *Cell Rep Med*. 2021;2(4):100242.
17 Sharma NS, Patel K, Sari E, et al. Active transcription in the vascular bed characterizes rapid progression in idiopathic pulmonary fibrosis. *J Clin Invest*. 2023;133(16).
18 Goda Y, Naito T, Banday MM, et al. Spatial transcriptomics reveals coordinated endothelial and epithelial activator protein-1 activation in chronic lung allograft dysfunction. *J Heart Lung Transplant*. 2026. https://doi.org/10.1016/j.healun.2026.01.028.
19 Ram-Mohan S, Bai Y, Schaible N, et al. Tissue traction microscopy to quantify muscle contraction within precision-cut lung slices. *Am J Physiol Lung Cell Mol Physiol*. 2020;318(2):L323–L330.
20 Khatri A, Todd JL, Kelly FL, et al. JAK-STAT activation contributes to cytotoxic T cell-mediated basal cell death in human chronic lung allograft dysfunction. *JCI Insight*. 2023;8(6).
21 Potter AS, Sharma NS, Goda Y, et al. Human lung allografts experience persistent fibrogenic shift following acute cellular rejection. *J Heart Lung Transplant*. 2026. https://doi.org/10.1016/j.healun.2026.02.1666.
22 Ning S, Pagano JS, Barber GN. IRF7: activation, regulation, modification and function. *Genes Immun*. 2011;12(6):399–414.
23 Eloranta ML, Franck-Larsson K, Lovgren T, et al. Type I interferon system activation and association with disease manifestations in systemic sclerosis. *Ann Rheum Dis*. 2010;69(7):1396–1402.
24 Valenzi E, Tabib T, Papazoglou A, et al. Disparate interferon signaling and shared aberrant basaloid cells in single-cell profiling of idiopathic pulmonary fibrosis and systemic sclerosis-associated interstitial lung disease. *Front Immunol*. 2021;12:595811.
25 Sun L, Zhu Z, Cheng N, Yan Q, Ye RD. Serum amyloid A induces interleukin-33 expression through an IRF7-dependent pathway. *Eur J Immunol*. 2014;44(7):2153–2164.
26 Wu M, Skaug B, Bi X, et al. Interferon regulatory factor 7 (IRF7) represents a link between inflammation and fibrosis in the pathogenesis of systemic sclerosis. *Ann Rheum Dis*. 2019;78(11):1583–1591.
27 Banday MM, Rao SB, Shankar S, et al. IL-33 mediates pseudomonas induced airway fibrogenesis and is associated with CLAD. *J Heart Lung Transplant*. 2023;42(1):53–63.
28 Kobayashi T, Kim H, Liu X, et al. Matrix metalloproteinase-9 activates TGF-beta and stimulates fibroblast contraction of collagen gels. *Am J Physiol Lung Cell Mol Physiol*. 2014;306(11):L1006–L1015.
29 Suga M, Iyonaga K, Okamoto T, et al. Characteristic elevation of matrix metalloproteinase activity in idiopathic interstitial pneumonias. *Am J Respir Crit Care Med*. 2000;162(5):1949–1956.
30 Liang Y, Yang N, Pan G, Jin B, Wang S, Ji W. Elevated IL-33 promotes expression of MMP2 and MMP9 via activating STAT3 in alveolar macrophages during LPS-induced acute lung injury. *Cell Mol Biol Lett*. 2018;23:52.
31 Allyn PR, Duffy EL, Humphries RM, et al. Graft loss and CLAD-onset is hastened by viral pneumonia after lung transplantation. *Transplantation*. 2016;100(11):2424–2431.
32 Jefferies CA. Regulating IRFs in IFN driven disease. *Front Immunol*. 2019;10:325.
33 Walker FC, Sridhar PR, Baldridge MT. Differential roles of interferons in innate responses to mucosal viral infections. *Trends Immunol*. 2021;42(11):1009–1023.
34 Iwasaki A, Pillai PS. Innate immunity to influenza virus infection. *Nat Rev Immunol*. 2014;14(5):315–328.
35 Sugiura H, Ichikawa T, Koarai A, et al. Activation of toll-like receptor 3 augments myofibroblast differentiation. *Am J Respir Cell Mol Biol*. 2009;40(6):654–662.
36 van Zoelen MA, van der Sluijs KF, Achouiti A, et al. Receptor for advanced glycation end products is detrimental during influenza A virus pneumonia. *Virology*. 2009;391(2):265–273.
37 Campbell TM, Liu Z, Zhang Q, et al. Respiratory viral infections in otherwise healthy humans with inherited IRF7 deficiency. *J Exp Med*. 2022;219(7).
38 Qing J, Liu C, Choy L, Wu RY, Pagano JS, Derynck R. Transforming growth factor beta/Smad3 signaling regulates IRF-7 function and transcriptional activation of the beta interferon promoter. *Mol Cell Biol*. 2004;24(3):1411–1425.
39 Brunner TM, Serve S, Marx AF, et al. A type 1 immunity-restricted promoter of the IL-33 receptor gene directs antiviral T-cell responses. *Nat Immunol*. 2024;25(2):256–267.
40 Polumuri SK, Jayakar GG, Shirey KA, et al. Transcriptional regulation of murine IL-33 by TLR and non-TLR agonists. *J Immunol*. 2012;189(1):50–60.
41 Ravanetti L, Dijkhuis A, Dekker T, et al. IL-33 drives influenza-induced asthma exacerbations by halting innate and adaptive antiviral immunity. *J Allergy Clin Immunol*. 2019;143(4):1355–1370.e16.
42 Wang Y, Jiao L, Qiang C, et al. The role of matrix metalloproteinase 9 in fibrosis diseases and its molecular mechanisms. *Biomed Pharmacother*. 2024;171:116116.
43 Ruigrok MJR, Maggan N, Willaert D, et al. siRNA-Mediated RNA interference in precision-cut tissue slices prepared from mouse lung and kidney. *AAPS J*. 2017;19(6):1855–1863.
44 Minaga K, Watanabe T, Arai Y, et al. Activation of interferon regulatory factor 7 in plasmacytoid dendritic cells promotes experimental autoimmune pancreatitis. *J Gastroenterol*. 2020;55(5):565–576.
45 Watanabe T, Yamashita K, Arai Y, et al. Chronic fibro-inflammatory responses in autoimmune pancreatitis depend on IFN-alpha and IL-33 produced by plasmacytoid dendritic cells. *J Immunol*. 2017;198(10):3886–3896.
46 Ma W, Huang G, Wang Z, Wang L, Gao Q. IRF7: role and regulation in immunity and autoimmunity. *Front Immunol*. 2023;14:1236923.
47 Liang H, Xu F, Wen XJ, et al. Interleukin-33 signaling contributes to renal fibrosis following ischemia reperfusion. *Eur J Pharmacol*. 2017;812:18–27.
48 Wu F, Zhang S, Zhuang R, Hu C, Zhu K. Blocking IL-33 decelerates cartilage degeneration in knee osteoarthritis through mice model. *PLoS One*. 2024;19(8):e0301199.
49 Ramirez AM, Shen Z, Ritzenthaler JD, Roman J. Myofibroblast transdifferentiation in obliterative bronchiolitis: tgf-beta signaling through smad3-dependent and -independent pathways. *Am J Transplant*. 2006;6(9):2080–2088.
50 Ramirez AM, Takagawa S, Sekosan M, Jaffe HA, Varga J, Roman J. Smad3 deficiency ameliorates experimental obliterative bronchiolitis in a heterotopic tracheal transplantation model. *Am J Pathol*. 2004;165(4):1223–1232.
51 Suwara MI, Vanaudenaerde BM, Verleden SE, et al. Mechanistic differences between phenotypes of chronic lung allograft dysfunction after lung transplantation. *Transpl Int*. 2014;27(8):857–867.
52 Renaud-Picard B, Moshkelgosha S, Berra G, et al. Detailed cellular and spatial characterization of chronic lung allograft dysfunction using imaging mass cytometry. *J Heart Lung Transplant*. 2025;44(1):118–124.